

The beta component of gamma-band auditory steady-state responses in patients with schizophrenia

Christoph Metzner^{1,2} and Volker Steuber²

¹Neural Information Processing Group, Institute of Software
Engineering and Theoretical Computer Science, Technische
Universität Berlin, Berlin, Germany

²Centre for Computer Science and Informatics Research,
University of Hertfordshire, Hatfield, United Kingdom

February 15, 2021

Abstract

The mechanisms underlying circuit dysfunctions in schizophrenia (SCZ) remain poorly understood. Auditory steady-state responses (ASSRs), especially in the gamma and beta band, have been suggested as a potential biomarker for SCZ. While the reduction of 40Hz power for 40Hz drive has been well established and replicated in SCZ patients, studies are inconclusive when it comes to an increase in 20Hz power during 40Hz drive. There might be several factors explaining the inconsistencies, including differences in the sensitivity of the recording modality (EEG vs MEG), differences in stimuli (click-trains vs amplitude-modulated tones) and large differences in the amplitude of the stimuli. Here, we used a computational model of ASSR deficits in SCZ and explored the effect of three SCZ-associated microcircuit alterations: reduced GABA activity, increased GABA decay times and NMDA receptor hypofunction. We investigated the effect of input strength on gamma (40 Hz) and beta (20 Hz) band power during gamma ASSR stimulation and saw that the pronounced increase in beta power during gamma stimulation seen experimentally could only be reproduced in the model when GABA decay times were increased and only for a specific range of input strengths. More specifically, when the input was in this specific range, the rhythmic drive at 40Hz produced a strong 40Hz rhythm in the control network; however, in the ‘SCZ-like’ network, the prolonged inhibition led to a so-called ‘beat-skipping’, where the network would only strongly respond to every other input. This mechanism was responsible for the emergence of the pronounced 20Hz beta peak in

the power spectrum. The other two microcircuit alterations were not able to produce a substantial 20 Hz component but they further narrowed the input strength range for which the network produced a beta component when combined with increased GABAergic decay times. Our finding that the beta component only existed for a specific range of input strengths might explain the seemingly inconsistent reporting in experimental studies and suggests that future ASSR studies should systematically explore different amplitudes of their stimuli. Furthermore, we provide a mechanistic link between a microcircuit alterations and an electrophysiological marker in schizophrenia and argue that more complex ASSR stimuli are needed to disentangle the nonlinear interactions of microcircuit alterations. The computational modelling approach put forward here is ideally suited to facilitate the development of such stimuli in a theory-based fashion.

1 Introduction

2 Auditory processing crucially relies on the fast temporal integration and resolution
3 of inputs to form coherent percepts. Gamma band oscillations (>30 Hz) have been
4 hypothesized to underlie this fast processing of auditory inputs [34, 33, 1] and, more
5 generally, to establish communication between distributed neuronal groups [8]. One
6 very simple way to test the ability of a neuronal microcircuit to generate and main-
7 tain oscillatory activity are steady-state responses (SSRs) - evoked oscillatory re-
8 sponses entrained to the frequency and phase of periodic stimuli. Importantly, pa-

9 tients with schizophrenia robustly show deficits in the 40-Hz auditory steady-state
10 responses (ASSRs) [37, 21] and this general oscillatory deficit has been implicated
11 in the pronounced perceptual and cognitive changes these patients experience [38].
12 This view is further underpinned by a large body of evidence documenting alterations
13 of parvalbumin-positive (PV⁺) γ -aminobutyric acid (GABA) interneurons and their
14 N-methyl-D-aspartate (NMDA) receptors [9, 10, 19, 22].

15 Interestingly, 50% of PV⁺ neurons in the dorsolateral prefrontal cortex of SCZ
16 patients have very low levels of the GAD67 isoform of glutamate decarboxylase [16].
17 This reduced expression of GAD67 mRNA has been demonstrated to decrease the
18 GABA synthesis in cortical GABAergic neurons, which would then result in smaller
19 amplitudes of inhibitory postsynaptic currents (IPSCs) [9]. Additionally, PV⁺ neurons
20 show reduced levels of the plasma membrane GABA transporter GAT1 in SCZ patients
21 [42]. A reduced concentration of GAT1 has been shown to increase the time GABA
22 molecules reside at the receptor and thus increase IPSC durations [32].

23 Administration of NMDAR antagonists lead to the emergence of schizophrenia-like
24 symptoms, such as hallucinations, delusions and thought disorder, in healthy subjects
25 [18]. Based on these findings it has been hypothesized that the reduced inhibition
26 found in SCZ might not be a consequence of the changes to PV⁺ neurons described
27 above, but could be attributable to an NMDAR hypofunction. Dysfunction of NM-
28 DARS in SCZ is supported by several lines of evidence [19]. Specifically, Carlen et al.
29 [7] found that targeted deletion of NMDARs from PV⁺ interneurons led to increased
30 spontaneous gamma oscillations and a deficit in gamma induction. Interestingly, they
31 could reproduce these results in an established circuit model [40] when they imple-

32 mented NMDAR hypofunction as an overall decrease in interneuron excitability.

33 In this study, we used an established network model of ASSR deficits in SCZ [40,
34 26], where SCZ-like behaviour is produced by an increase in IPSC decay times, to
35 examine the dependence of 40 Hz ASSRs on the strength or amplitude of the inputs.
36 In our model we could only reproduce the emergence of 20 Hz component during 40 Hz
37 stimulation seen experimentally if the input strength was in a narrow range. More
38 specifically, very weak input to the network did not result in a pronounced oscillatory
39 rhythm. When the input was in a specific range, the 40 Hz stimulation entrained a
40 pure 40 Hz oscillation in the control network, whereas in the ‘SCZ-like’ network, the
41 changed IPSC time course caused a so-called ‘beat-skipping’, where the network would
42 only strongly respond to every other input. This resulted in significant increase in 20 Hz
43 power. Ultimately, if the input became too strong, the increased IPSC decay time was
44 insufficient to suppress the very strong 40 Hz input. This was reflected in a single peak
45 at 40Hz in the power spectrum. We then extended the network model to include more
46 cellular-level alterations such as reduced GABA levels and NMDAR hypofunction.
47 We found that the addition of further alterations did not change the input strength
48 dependence of the 20 Hz component but further limited the parameter range where
49 the component would occur. Our finding that the beta component only existed for
50 a specific range of input strengths might explain the seemingly inconsistent reporting
51 in experimental studies and suggests that future ASSR studies should systematically
52 explore different amplitudes of their stimuli.

53 In this study, we used an established network model of ASSR deficits in SCZ [40, 26],
54 where SCZ-like behaviour is produced in the model by an increase in IPSC decay times,

55 to examine the dependence of 40 Hz ASSRs on the strength or amplitude of the inputs.
56 We found that the pronounced increase in 20 Hz power during 40 Hz stimulation seen
57 experimentally could only be reproduced in the model for a specific range of input
58 strengths. More specifically, if the input was too weak the network failed to produce
59 a strong oscillatory rhythm. When the input was in the specific range, the rhythmic
60 drive at 40 Hz produced a strong 40 Hz rhythm in the control network, however, in
61 the ‘SCZ-like’ network, the prolonged inhibition led to a so-called ‘beat-skipping’,
62 where the network would only strongly respond to every other input. This mechanism
63 was responsible for the emergence of the pronounced 20 Hz beta peak in the power
64 spectrum. However, if the input exceeded a certain strength value, the 20 Hz peak in
65 the power spectrum disappeared again. In this case, prolonged inhibition due to the
66 increased IPSC decay times was insufficient to suppress the now stronger gamma drive
67 from the input, resulting in an absence of the beat-skipping and single peak at 40 Hz
68 in the power spectrum. We then extended the network model to include more cellular-
69 level alterations such as reduced GABA levels and NMDAR hypofunction. We found
70 that the addition of further alterations did not change the input strength dependence
71 of the 20 Hz component but further limited the parameter range where the component
72 would occur. Our finding that the beta component only existed for a specific range
73 of input strengths might explain the seemingly inconsistent reporting in experimental
74 studies and suggests that future ASSR studies should systematically explore different
75 amplitudes of their stimuli.

76 2 Methods

77 The model proposed here is based on a recent reimplementation [26] of the simple
78 model presented by Vierling-Claassen et al. [40], which has been used in previous
79 studies of ASSR deficits [30], and which is integrated in the ASSRUnit model database,
80 a framework for automated testing of ASSR models against observations from empirical
81 studies [28].

82 Single Cell Model

83 Single cells are represented as theta neurons (see e.g. [4] for an in-depth analysis and
84 description of the theta neuron model).

85 The k th neuron in a network is described by the variable θ_k , which represents the
86 neuron state, and which is governed by the following equation

$$\frac{d\theta_k}{dt} = 1 - \cos \theta_k + (b + S_k + N(t))(1 + \cos \theta_k)$$

87 where b is an externally applied current, S is the total synaptic input to the cell
88 and $N(t)$ is a time-varying noise input. The total synaptic input to a cell in a network
89 amounts to

$$S_k = \sum_{j=1}^n \alpha_j g_{jk} s_{jk}$$

90 where n is the number of presynaptic neurons, α_j controls excitation and inhibition,
91 i.e. is $+1$ for excitatory synapses and -1 for inhibitory ones, g_{jk} is the synaptic
92 strength from cell j to cell k and s_{jk} is the synaptic gating variable from cell j to cell
93 k . Synaptic gating variables evolve according to

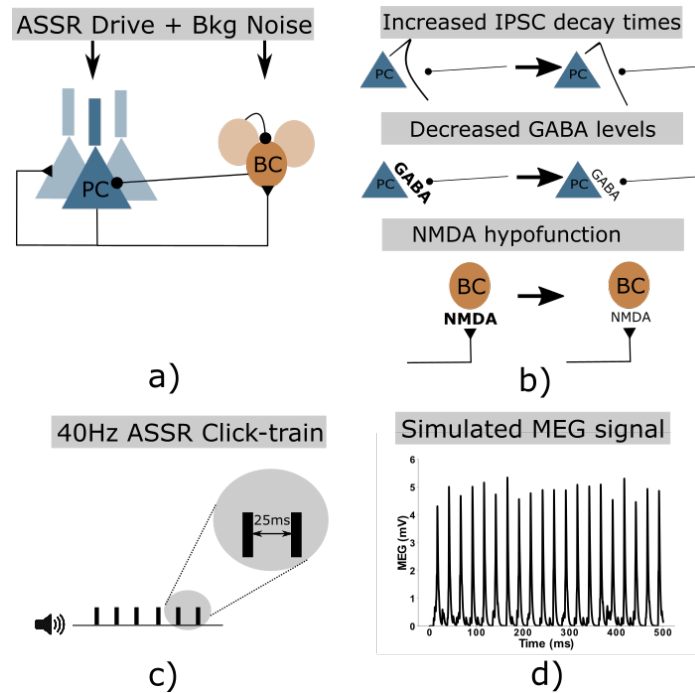


Figure 1: a) Network schematic showing the two neural populations (excitatory pyramidal cells and inhibitory basket cells) and their connectivity. Additionally, both populations receive periodic ASSR input drive and random background noise. b) Three potential microscopic changes underlying gamma ASSR deficits were implemented: Increased IPSC decay times at inhibitory synapses onto PCs, decreased GABA levels resulting in reduced IPSC amplitudes at inhibitory synapses onto PCs, NMDAR hypofunction resulting in decreased excitability of GABAergic interneurons c) Depiction of a 40 Hz click-train stimulus, where tones (synchronous inputs to the cells of the network) are presented with an inter-click interval of 25 ms resulting in a drive frequency of 40 Hz. d) Example simulated MEG signal of the network in response to a 40 Hz click-train stimulus.

Table 1: Model parameters

Parameter	Definition	Value
n_E	Exc. population size	20
n_I	Inh. population size	10
τ_R	Synaptic rise time	0.1
τ_{exc}	Excitatory decay time	2.0
τ_{inh}	Inhibitory decay time	8.0
g_{ee}	E-E synaptic strength	0.015
g_{ei}	E-I synaptic strength	0.025
g_{ie}	I-E synaptic strength	0.015
g_{ii}	I-I synaptic strength	0.02
g_{de}	Synaptic strength of drive to E cells	0.3
g_{di}	Synaptic strength of drive to I cells	0.08
I	Input strength factor (multiplied with g_{de} and g_{di})	varied (default=1.0)
b	Applied current (regardless of cell type)	-0.1
Ag_{max}	Scaling factor for noise EPSCs	0.6

$$\frac{ds_{jk}}{dt} = -\frac{s_{jk}}{\tau_j} + e^{-\eta(1+\cos\theta_j)} \frac{1-s_{jk}}{\tau_R}$$

94 where τ_j is the synaptic decay time, τ_R the synaptic rise time and η is a scaling
95 parameter. A single pacemaker cell provides rhythmic ASSR drive to the network.
96 Additionally, Poissonian noise input is also given to all cells in the network, where a
97 noise spike at time t_n elicits the following excitatory postsynaptic potential (EPSP)
98 $N(t)$

$$N(t) = H(t - t_n) \cdot \frac{Ag_{gmax}(e^{-(t-t_n)/\tau_{exc}} - e^{-(t-t_n)/\tau_R})}{\tau_{exc} - \tau_R}$$

99 where Ag_{gmax} is the noise strength, τ_{exc} is the synaptic decay time, τ_R the synaptic
100 rise time, and H the Heaviside function.

101 Network

102 We combined 20 excitatory pyramidal cells together with 10 inhibitory cells into a
103 network model, following the earlier work of [40, 26].

104 A schematic depiction of the network can be found in Figure 1. Populations connect
105 to each other and also to themselves. The connectivity between any two populations
106 is all-to-all. All populations also have two sources of input, the oscillatory drive input
107 and a background noise input. The drive input periodically sends spikes with a given
108 drive frequency to all populations, mimicking the rhythmic ASSR input. An overview
109 of the model parameters can be found in Table 1.

110 To evaluate the oscillatory entrainment we calculate simulated EEG/MEG signals
111 by summing all excitatory synaptic variables over all pyramidal cells (as in [40, 26,

112 30)). As the main measures for entrainment we perform a Fourier transform on these
113 ‘EEG/MEG’ signals and extract the power at 40 Hz and at 20 Hz.

114 **Implementation of schizophrenogenic microcircuit alterations**

115 We implemented changes to the GABAergic and glutamatergic neurotransmitter sys-
116 tems that have been associated with schizophrenia.

117 **GABAergic system** 50% of PV⁺ neurons in the dorsolateral prefrontal cortex lack
118 detectable levels of GAD67 [16]. It has been suggested that the reduced expression of
119 GAD67 mRNA likely implies a reduction in GABA synthesis in cortical GABAergic
120 neurons, which in turn would lead to smaller amplitude IPSCs at the postsynaptic site
121 [9]. We implemented this change as a reduction of the weight of inhibitory connections
122 (for both I-E and I-I connections).

123 Furthermore, a reduction in the plasma membrane GABA transporter GAT1 [32] has
124 also been found in PV⁺ interneurons in SCZ patients [42]. GAT1 is a major contributor
125 to the specificity of synapses by preventing spillover to neighbouring synapses [32] and
126 a reduction in GAT1 results in prolonged IPSC durations [32]. Here, we realised this
127 change as an increase of the IPSC decay time constant (as in previous studies [40, 26]).

128 **Glutamatergic system** NMDAR antagonists, such as phencyclidine and ketamine,
129 produce symptoms, which are very similar to key clinical features of SCZ [18]. Con-
130 vergent lines of evidence underpin that NMDARs are dysfunctional in SCZ [19]. Exam-
131 ples of direct evidence in favour of this hypothesis are changes in NMDAR-associated
132 protein levels at the postsynaptic site [3], a reduction in NMDAR-mediated signalling

133 following neuregulin 1 activation of ErbB4 receptors [11], lower levels of glutathione
134 (a modulator at the redox-sensitive site of NMDARs) [36] and a reduction of kynure-
135 nine 3-monooxygenase that might increase kynurenic acid (an NMDAR antagonist)
136 levels [41]. Indirect evidence, such as findings that putative risk genes for SCZ can
137 affect NMDAR function [13] and that substances enhancing NMDARs might reduce
138 symptom severity in SCZ [24], further underpin this idea. A potential hypofunction of
139 NMDARs would lead to lower levels of excitation of PV⁺ interneurons and we there-
140 fore implemented this alterations by decreasing the applied current b_{inh} to inhibitory
141 cells.

142 In this study, we considered four different 'SCZ-like' networks, which comprised
143 the following combinations of changes to the GABAergic and glutamatergic system
144 described above:

- 145 • *IPSC-SCZ-like* network: For this 'SCZ-like' network, we only implemented the
146 increase of the IPSC decay time constant (as in previous studies [40, 26]).
- 147 • *IPSC+gGABA-SCZ-like* network: Here, additionally to the increase of IPSC
148 decay times, we also reduced the weight of the inhibitory GABAergic connections
149 (as in other previous studies [29]).
- 150 • *IPSC+bInh-SCZ-like* network: For this network, we decreased the applied cur-
151 rent to the inhibitory cells together with the increase in IPSC decay times.
- 152 • *Full-SCZ-like* network: Here, we combined all three alterations, i.e. we imple-
153 mented an increase in IPSC decay times, a decrease in inhibitory weights and a
154 decrease in applied currents to inhibitory cells.

155 **Implementation details and code availability**

156 The model was implemented using Python 2.7.9 and numpy 1.9.3. Analysis and visu-
157 alization of the model output was also done in Python using the numpy and matplotlib
158 packages (matplotlib 1.4.3).

159 Model equations were numerically solved using a simple forward Euler scheme. A
160 single model run simulated a 500 ms trial and the time step was chosen such that
161 this resulted in $2^{13} = 8192$ data points. The model output was unaffected by using a
162 smaller time step.

163 Simulation results varied from trial to trial because of the stochastic nature of the
164 background input. Therefore, we always performed 20 simulation trials, each with a
165 different realisation of the noise process. We then averaged these trials in time to get
166 an average simulated MEG signal and all analyses were based on this average signal.

167 Model and analysis code are available on GitHub ([https://github.com/ChristophMetzner/Gamma-](https://github.com/ChristophMetzner/Gamma-Input-Dependence)
168 [Input-Dependence](https://github.com/ChristophMetzner/Gamma-Input-Dependence)) and the model will be submitted to ModelDB (<https://senselab.med.yale.edu/modeldb/>)
169 upon publication.

170 **3 Results**

171 **Replication of previous findings** First, we validated the *IPSC-SCZ-like* model against
172 experimental observations [40] and replicated the findings from previous modelling
173 studies with this model [40, 26]. The control network strongly entrains to the driving
174 stimulus, regardless of the specific driving frequency (Figures 2 and 3 left columns),
175 and shows stronger entrainment at 40 Hz than for 30 and 20 Hz, consistent with exper-

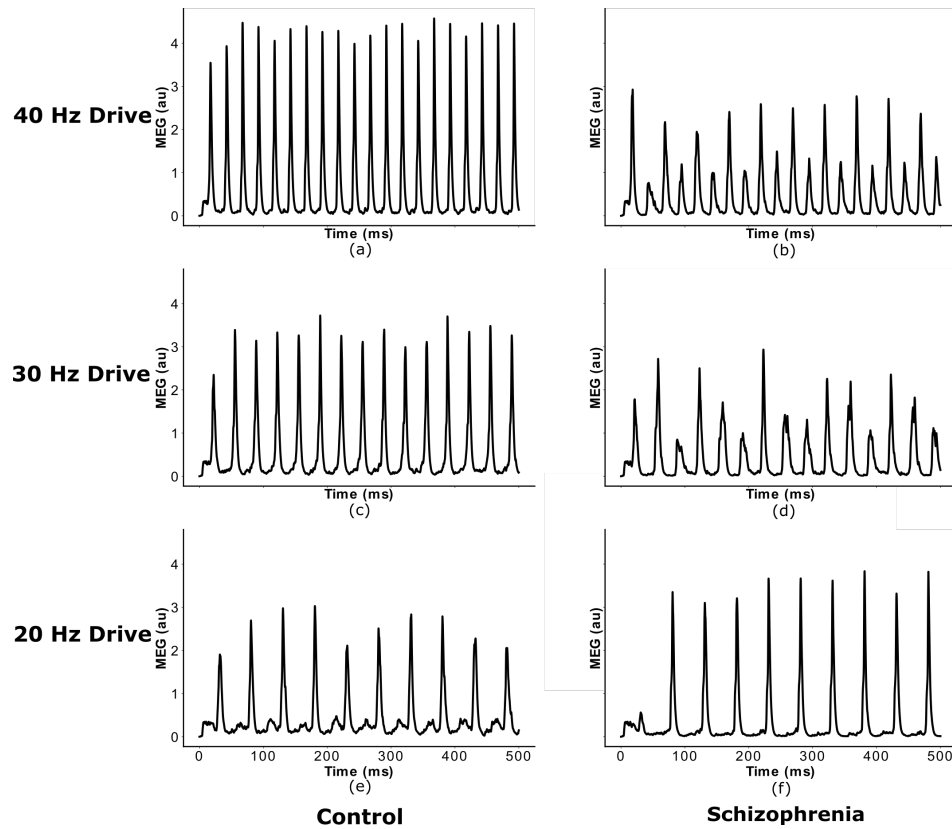


Figure 2: **Network response to ASSR stimuli of different frequency.** Simulated MEG signal of the control and *IPSC-SCZ-like* network in response to click-train stimuli with drive frequencies of 20, 30, and 40 Hz, replicating earlier studies using this model [40, 26].

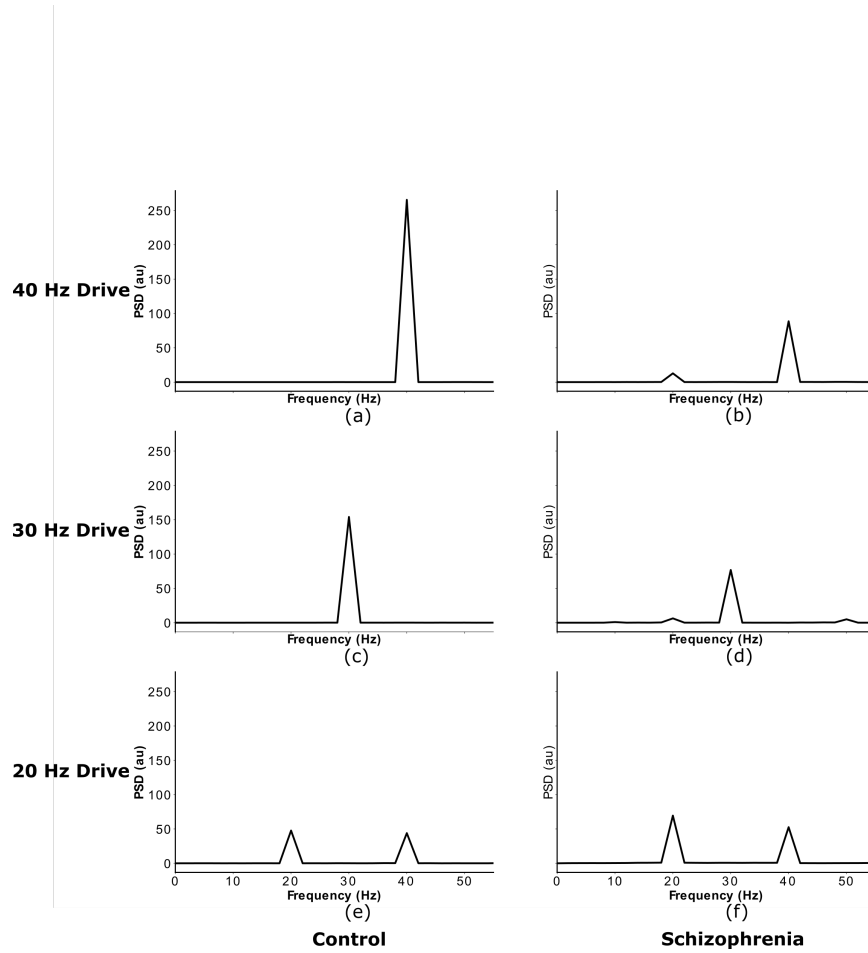


Figure 3: **Power spectra of network responses to ASSR stimuli of different frequency.** Power spectral densities of the simulated MEG signals from Figure 2, again replicating earlier studies using this model [40, 26].

176 iments [40]. Furthermore, the control model replicates another important feature seen
177 in experiments and the previous models, a strong 40 Hz component for 20 Hz drive
178 (Figures 2 and 3 left columns, third rows). The 'SCZ-like' network, where 'SCZ-like'
179 behaviour is achieved by an increase in the GABAergic IPSC decay time constant
180 (from 8 ms to 28 ms as in earlier studies), also reproduces important characteristics
181 from experiments and previous models: First, the 'IPSC-SCZ-like' network shows a
182 marked reduction in 40 Hz power for 40 Hz drive (Figure 3, right column, first row),
183 as previously found in experiments (see [37] for a meta-analysis) and models [40, 26].
184 Furthermore, this network shows an emergent 20 Hz component at 40 Hz drive (Figure
185 3, right column, first row) as seen in [21, 40, 26] but not in other experimental studies
186 [37]; and we see an increase in 20 Hz power and a relative decrease in 40 Hz power for
187 20 Hz drive in this condition (Figure 3, right column, third row).

188 **Input Strength Dependence of the 20 Hz Component** Next, we explored the input
189 strength dependence of the *IPSC-SCZ-like* model response to 40 Hz drive by multi-
190 plying the input strength of the SCZ model by factors ranging from 0.1 to 1.5 in
191 steps of 0.1. Figure 4 a) shows that the 40 Hz power increases with increasing input
192 strength. Figure 4 b) shows that the 20 Hz component emerges at an input strength
193 of 80% of the default strength, sharply increases for stronger inputs around the the
194 default SCZ network strength and then sharply decreases again for inputs of 120% of
195 the default strength and higher. Thus, in a narrow range between 80 and 120% of the
196 default inhibitory input strength the network response exhibits a shift of power from
197 the gamma (40 Hz) to the beta (20 Hz) band. Figures 4 c) and f) and Supplementary

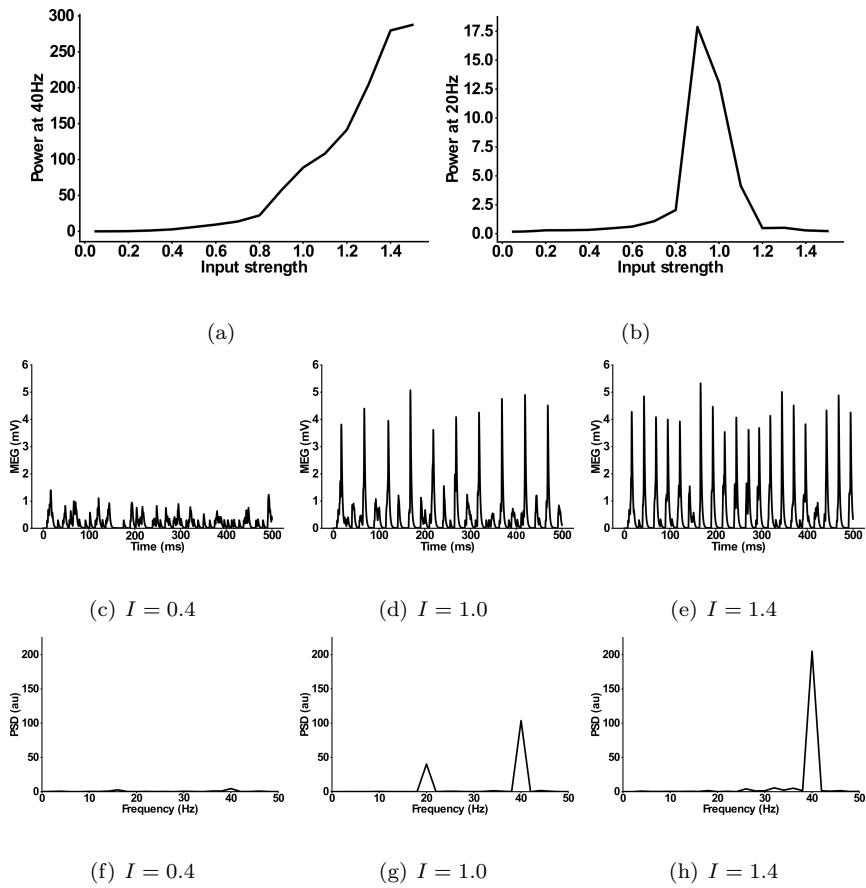


Figure 4: **Input dependence of the 20 Hz component in the 'IPSC-SCZ-like'**

model (a) Power at 40 Hz in response to 40 Hz drive as a function of the input strength. (b) Power at 20 Hz in response to 40 Hz drive as a function of the input strength. (c-e) Simulated MEG signals for three different input strengths: (c) $I = 0.4$ Input strength too low to drive synchronization. (d) $I = 1.0$ Input strength high enough to drive synchronization and to allow for a beat-skipping behaviour. (e) $I = 1.4$ Input strength too strong for beat-skipping behaviour, external 40 Hz drive dominates recurrent effects. (f-h) Power spectral densities for the signals from (c-e).

198 Figure 10 a) show that for weak inputs the oscillatory drive is not strong enough force
199 the network into a coherent rhythm and, therefore, the powers at 40 Hz and at 20 Hz
200 are very low. For input strengths around the default SCZ network value, the input
201 strongly drives the network and forces it into a rhythm. However, the increased IPSC
202 decay times prevent the excitatory pyramidal neurons from responding to every 40 Hz
203 cycle and only allow them to spike every other cycle (Figures 4 d) and g) and Supple-
204 mentary Figure 10 b)). Thus, the network rhythm displays a so-called 'beat-skipping'
205 behaviour. The power spectrum of the response therefore shows both a 40 Hz (which is
206 substantially smaller than for the control network) and a prominent 20 Hz peak (which
207 is not visible for the control network). If the input, however, exceeds 120% of the de-
208 fault SCZ network value, the rhythmic input becomes strong enough to overcome the
209 prolonged inhibition and forces the network into a gamma oscillation at 40 Hz. Here,
210 the excitatory cells fire during each cycle and the power spectrum only shows a large
211 40 Hz peak (Figures 4 e) and h) and Supplementary Figure 10 c)).

212 **Combinations of Alterations and their Input-Strength-Dependence** As explained
213 earlier it is unlikely that the microscopic alterations associated with schizophrenia
214 occur in isolation. Therefore, we added two more alterations to the *IPSC-SCZ-like*
215 model: 1) A reduction in GABA levels, implemented as a reduction of the inhibitory
216 weights; 2) A hypofunction of NMDARs at inhibitory interneurons, implemented as a
217 reduction in interneuron excitability. We first added these modifications individually
218 and combined them in a final set of simulations.

219 For the *IPSC+gGABA-SCZ-like* model, which included different GABA levels, we

220 can see in Figure 5 that the 40 Hz component is shifted to lower input strengths
221 and slightly decreased in power for low levels of GABA, but that the main effect is
222 on the 20 Hz component. However, the emergent 20 Hz component, which existed
223 for a narrow input strength range for the *IPSC-SCZ-like* model, narrowed down and
224 finally vanished for stronger reductions of GABA levels. For the *IPSC+bInh-SCZ-*
225 *like* model, with NMDAR hypofunction, the input strength dependence of the 40 Hz
226 component exhibited a shift to lower input strengths than the model without NMDA
227 receptor hypofunction and the 20 Hz component only emerged for weak reductions
228 of the interneuron excitability (Figure 6). Lastly, the full model combining all three
229 alterations, displayed similar behaviour as the previous models but an even more
230 pronounced shift of the 40 Hz components to lower input strengths for higher levels of
231 GABA (Figure 7).

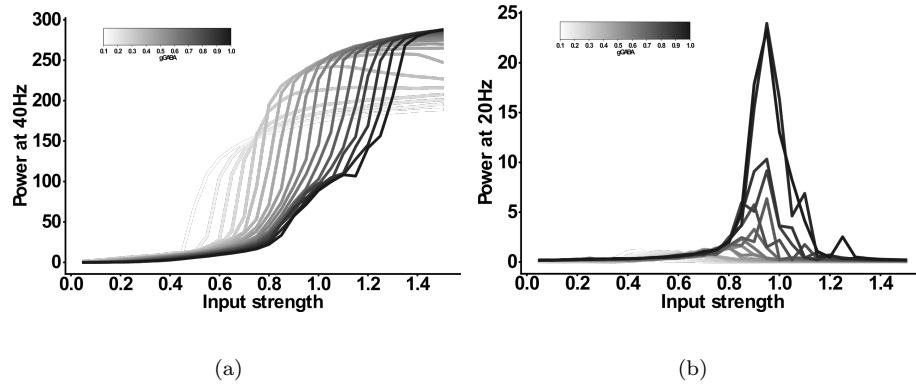


Figure 5: **Input strength dependence of the 20 Hz component in the 'IPSC+gGABA-SCZ-like' model.** (a) Power at 40 Hz in response to 40 Hz drive as a function of the input strength. (b) Power at 20 Hz in response to 40 Hz drive as a function of the input strength. In both plots the network model has increased IPSC decay times (from 8 ms to 28 ms) and the I-E and I-I synaptic strength (g_{ie} and g_{ii} , respectively) is varied from 100% (black) to 10% (lightest grey) in steps of 5%.

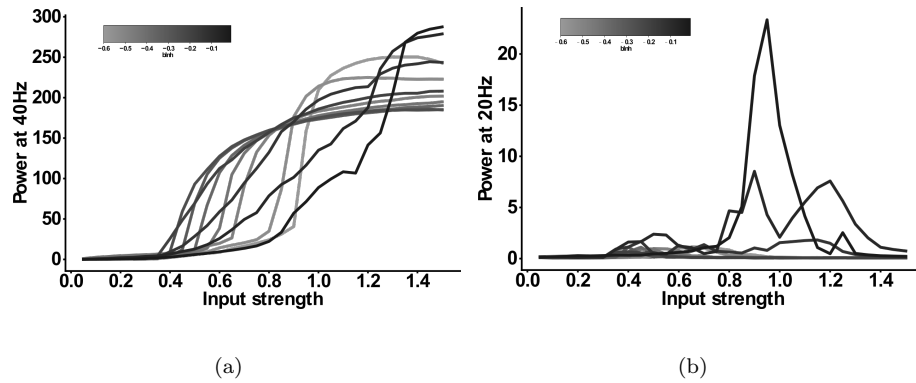


Figure 6: **Input strength dependence of the 20 Hz component 'IPSC+bInh-SCZ-like' model.** (a) Power at 40 Hz in response to 40 Hz drive as a function of the input strength. (b) Power at 20 Hz in response to 40 Hz drive as a function of the input strength. In both plots the network model has increased IPSC decay times (from 8 ms to 28 ms) and the interneuron excitability b_{inh} is varied from -0.01 (black) to -0.1 (darkest grey) and then in steps of -0.05 to -0.6 (lightest grey).

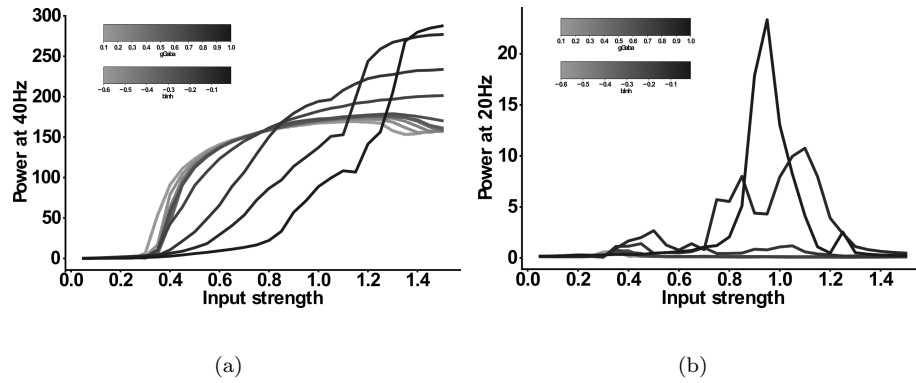


Figure 7: **Input strength dependence of the 20 Hz component 'Full-SCZ-like'**

model. (a) Power at 40 Hz in response to 40 Hz drive as a function of the input strength. (b) Power at 20 Hz in response to 40 Hz drive as a function of the input strength. In both plots the network model has increased IPSC decay times (from 8 ms to 28 ms) and now both the I-E and I-I synaptic strength (g_{ie} and g_{ii} , respectively) is varied from 100% (black) to 10% (lightest grey) in steps of 10% and simultaneously the interneuron excitability b_{inh} is varied from -0.01 (black) to -0.1 (darkest grey) and then in steps of -0.05 to -0.6 (lightest grey).

232 4 Discussion

233 Whether the presence of a 20 Hz beta response component in EEG/MEG signals for
234 40 Hz gamma drive during auditory steady state responses is an indicator of schizophre-
235 nia currently remains unresolved. In the present computational modelling study, we
236 explored the conditions leading to the emergence of such a 20 Hz component. We could
237 demonstrate that: (a) this beta component was only present in models that include an
238 increased IPSC decay time but not in models that solely modelled decreased GABA
239 activity or NMDAR hypofunction, further confirming the initial findings of Vierling-
240 Claassen et al. [40], (b) the component strongly depended on the input strength and
241 (c) the addition of GABA activity or NMDAR deficits to the IPSC decay time increases
242 further narrowed the range of input strengths for which a substantial beta component
243 existed. These results explain the seemingly inconsistent findings regarding the beta
244 component of the 40 Hz ASSR measure in the literature.

245 However, there are several other potential factors that could contribute to these
246 inconsistent experimental results. First, a difference in stimuli might play a role,
247 since some studies use amplitude-modulated tones as opposed to the click-trains used
248 in Vierling-Claassen et al. [40]. Second, most ASSR studies are performed using
249 EEG recordings and the lower sensitivity of EEG compared to MEG might explain
250 why the more subtle effect of the beta component has not been detected with EEG.
251 Furthermore, as already pointed out by Vierling-Claassen et al. [40], averaging in time
252 before the transformation into the frequency domain can potentially reduce the 20 Hz
253 component considerably since the beat-skipping behaviour can vary from trial to trial.

254 The skipped beats can be the 1st, 3rd, 5th,... in one trial while being the 2nd, 4th,
255 6th,.. in another trial, and thus would cancel out when averaged over in time prior
256 to the frequency transform. Nevertheless, our modelling results offer a plausible and
257 simple explanation of the inconsistent experimental results and suggest a careful choice
258 of the input strengths in ASSR experiments.

259 We used a simple computational model consisting of an excitatory population, rep-
260 resenting pyramidal cells, and an inhibitory population, representing PV⁺ inhibitory
261 interneurons. While most of the experimental evidence for a reduction in GAT1, which
262 in turn would lead to an increase in IPSC decay times, points towards chandelier cells
263 [23], we have previously shown that at realistically low ratios of chandelier cells to
264 basket cells in a microcircuit, gamma and beta range ASSR changes as seen in SCZ
265 patients, are most likely due to an increase of IPSC decay times at basket cell synapses
266 [30]. Our simplified model does not incorporate other types of inhibitory interneurons
267 such as somatostatin-positive (SST⁺) or vasoactive intestinal peptide-positive (VIP⁺),
268 although they have been shown to play important functional roles in cortical micro-
269 circuits [5]. Furthermore, there is recent experimental evidence of alterations to SST⁺
270 interneurons in schizophrenia. Hashimoto et al. [14] found a reduced expression of
271 GAD67 in SST⁺ neurons, while no reduction of GAT1 was apparent. Furthermore,
272 Morris et al. [31] observed that both the density of SST neurons and the expression
273 of SST⁺ per neuron was reduced in schizophrenia. These changes have been found in
274 most cortical layers with varying strength [31] and can be observed throughout cortex
275 [15]. This suggests, however, that IPSC decay times at SST⁺ interneuron synapses,
276 a necessary requirement for the emergence of a beta component in our model, should

277 remain intact in patients with schizophrenia. Additionally, the generation and mainte-
278 nance of fast cortical rhythms in the beta and gamma range has been mainly attributed
279 to PV⁺ neurons [12, 2, 6], although SST⁺ neurons have recently also been found to be
280 involved [39]. These findings suggest that alterations of SST⁺ interneurons should only
281 play a minor role in the emergence of a beta component in gamma ASSR tasks, and
282 they were therefore not considered in the present study. Nevertheless, an exploration
283 of the effects of SST⁺ alterations on cortical rhythms, especially for the lower fre-
284 quency bands such as theta and alpha and for theta-gamma cross-frequency coupling,
285 is warranted.

286 Beyond the question whether a beta component emerges in ASSR responses of pa-
287 tients with schizophrenia or not, our modelling work addresses a broader and more
288 important issue. In general, it has proven extremely difficult to map schizophrenia-
289 associated alterations of local microcircuits to specific neurocognitive or electrophys-
290 iological markers. Similar difficulties exist for other neuropsychiatric disorders such
291 as autism spectrum disorder. Our work here shows that, while the robust deficit in
292 the 40 Hz response to 40 Hz drive is not specific to a single microcircuit alteration, the
293 emergence of the 20 Hz is. The computational model presented here mechanistically
294 links the microcircuit change to the electrophysiological marker, thus, demonstrating
295 the usefulness of mechanistic computational models in advancing our understanding
296 of the relationship between features of the microcircuitry and non-invasive biomark-
297 ers, as we have argued before [25]. Furthermore, our simulation results show that the
298 standard 40 Hz ASSR measure is not specific enough to resolve the complex, nonlin-
299 ear interactions on the local circuit level and that more complex experimental designs

300 are needed to disentangle them. This becomes especially important when considering
301 that not only changes to the glutamatergic and GABAergic synapses considered in this
302 work influence gamma ASSRs, but also neuromodulators such as dopamine [20] and
303 cell-intrinsic changes to voltage-gated ionic channels [27]. This is further underpinned
304 by the low specificity of the 40 Hz ASSR to schizophrenia, as for example similar ASSR
305 deficits have been found in autism spectrum disorder [35] and bipolar disorder [17].

306 In summary, with this computational study we provide insights into the mechanistic
307 generation of ASSR frequency components in schizophrenia beyond the traditional
308 40 Hz power at 40 Hz drive. Furthermore, we are able to explain seemingly conflicting
309 experimental findings and suggest a more thorough and careful consideration of the
310 effect of stimulus strength when designing ASSR experiments. Finally, we argue for
311 a more complex and model-driven design of gamma and beta ASSR experiments in
312 schizophrenia and for other neuropsychiatric disorders, which might be better suited
313 to disentangle the nonlinear contributions of different microcircuit alterations found
314 in these disorders.

315 **Supplementary Figures**

316 **Reduced GABA levels**

317 Here, we explore the effect of potentially reduced GABAergic conductances as a con-
318 sequence of lower expression of GAD67 on the 40 and 20 Hz power at 40 Hz drive.

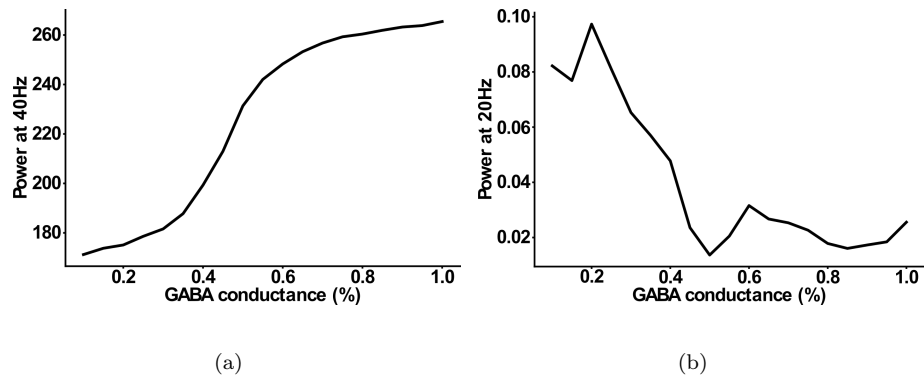


Figure 8: **Effect of reduced GABAergic synaptic strength.** (a) Power at 40 Hz in response to 40 Hz drive as a function of GABAergic synaptic strength. (b) Power at 20 Hz in response to 40 Hz drive as a function of GABAergic synaptic strength.

319 **NMDA hypofunction**

320 Here, we explore the effect of potential NMDAR hypofunction on the 40 and 20 Hz
321 power at 40 Hz drive.

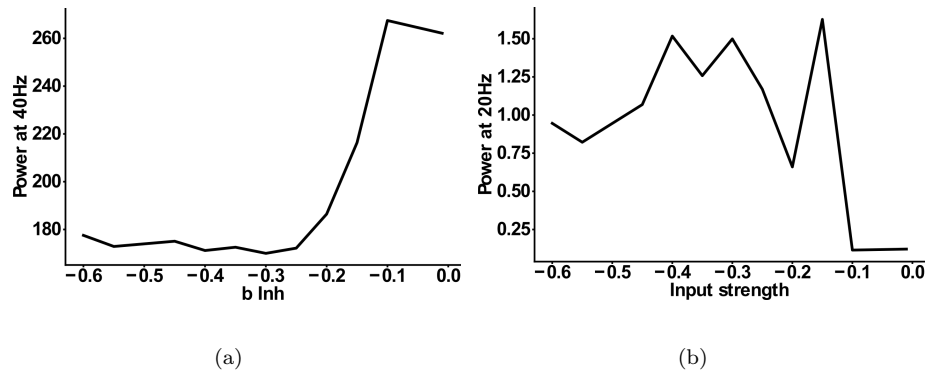
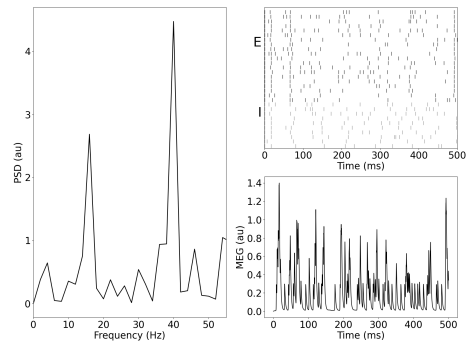


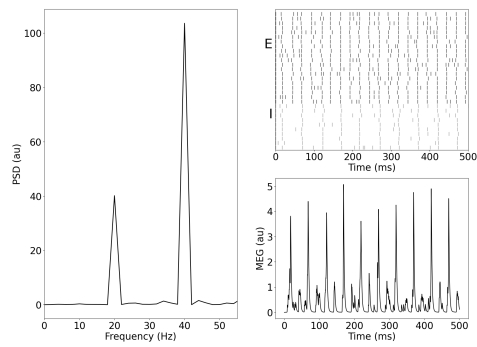
Figure 9: **Effect of reduced interneuron excitability.** (a) Power at 40 Hz in response to 40 Hz drive as a function of interneuron excitability. (b) Power at 20 Hz in response to 40 Hz drive as a function of interneuron excitability.

322 **Input Dependence**

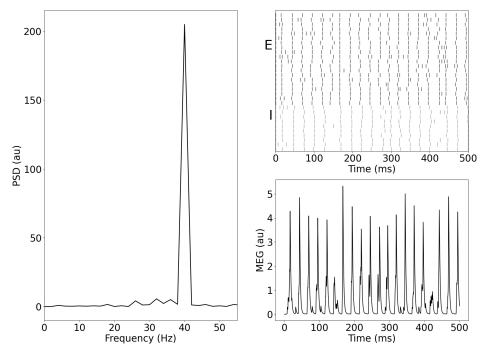
323 Example single model trials for the IPSC model in three different regions of the in-
324 put strength parameter space: below the critical range for the emergence of a 20 Hz
325 component (10 (a)), within this range (10 (b)) and above (10 (c)).



(a)



(b)



(c)

Figure 10: **Single model trials.** (a) Power spectral density, simulated MEG signal and raster plot for the IPSC model with an input strength of $I = 0.4$. (b) Same as (a) but for $I = 1.0$. (c) Same as (a) but for $I = 1.4$.

326 References

- 327 [1] Alina Baltus and Christoph Siegfried Herrmann. Auditory temporal resolution
328 is linked to resonance frequency of the auditory cortex. *International Journal of*
329 *Psychophysiology*, 98(1):1–7, 2015.
- 330 [2] Marlene Bartos, Imre Vida, and Peter Jonas. Synaptic mechanisms of synchro-
331 nized gamma oscillations in inhibitory interneuron networks. *Nature reviews neu-*
332 *roscience*, 8(1):45–56, 2007.
- 333 [3] Monica Beneyto and James H Meador-Woodruff. Lamina-specific abnormalities of
334 nmda receptor-associated postsynaptic protein transcripts in the prefrontal cortex
335 in schizophrenia and bipolar disorder. *Neuropsychopharmacology*, 33(9):2175–
336 2186, 2008.
- 337 [4] Christoph Börgers and Nancy Kopell. Synchronization in networks of excitatory
338 and inhibitory neurons with sparse, random connectivity. *Neural computation*,
339 15(3):509–538, 2003.
- 340 [5] Jessica A Cardin. Functional flexibility in cortical circuits. *Current opinion in*
341 *neurobiology*, 58:175–180, 2019.
- 342 [6] Jessica A Cardin, Marie Carlén, Konstantinos Meletis, Ulf Knoblich, Feng Zhang,
343 Karl Deisseroth, Li-Huei Tsai, and Christopher I Moore. Driving fast-spiking cells
344 induces gamma rhythm and controls sensory responses. *Nature*, 459(7247):663–
345 667, 2009.

- 346 [7] Marie Carlen, Konstantinos Meletis, JH Siegle, JA Cardin, Kensuke Futai, Dorea
347 Vierling-Claassen, Charlotta Ruehlmann, Stephanie R Jones, Karl Deisseroth,
348 MIMC Sheng, et al. A critical role for nmda receptors in parvalbumin interneurons
349 for gamma rhythm induction and behavior. *Molecular psychiatry*, 17(5):537–548,
350 2012.
- 351 [8] Pascal Fries. Rhythms for cognition: communication through coherence. *Neuron*,
352 88(1):220–235, 2015.
- 353 [9] Guillermo Gonzalez-Burgos and David A Lewis. Gaba neurons and the mecha-
354 nisms of network oscillations: implications for understanding cortical dysfunction
355 in schizophrenia. *Schizophrenia bulletin*, 34(5):944–961, 2008.
- 356 [10] Guillermo Gonzalez-Burgos and David A Lewis. Nmda receptor hypofunction,
357 parvalbumin-positive neurons, and cortical gamma oscillations in schizophrenia.
358 *Schizophrenia bulletin*, 38(5):950–957, 2012.
- 359 [11] Chang-Gyu Hahn, Hoau-Yan Wang, Dan-Sung Cho, Konrad Talbot, Raquel E
360 Gur, Wade H Berrettini, Kalindi Bakshi, Joshua Kamins, Karin E Borgmann-
361 Winter, Steven J Siegel, et al. Altered neuregulin 1–erbb4 signaling contributes
362 to nmda ζ receptor hypofunction in schizophrenia. *Nature medicine*, 12(7):824–
363 828, 2006.
- 364 [12] Norbert Hájos, János Pálhalmi, Edward O Mann, Beáta Németh, Ole Paulsen,
365 and Tamas F Freund. Spike timing of distinct types of gabaergic interneu-

366 ron during hippocampal gamma oscillations in vitro. *Journal of Neuroscience*,
367 24(41):9127–9137, 2004.

368 [13] Paul J Harrison and Daniel R Weinberger. Schizophrenia genes, gene expression,
369 and neuropathology: on the matter of their convergence. *Molecular psychiatry*,
370 10(1):40–68, 2005.

371 [14] Takanori Hashimoto, Dominique Arion, T Unger, JG Maldonado-Aviles, HM Mor-
372 ris, DW Volk, K Mirnics, and DA Lewis. Alterations in gaba-related transcriptome
373 in the dorsolateral prefrontal cortex of subjects with schizophrenia. *Molecular*
374 *psychiatry*, 13(2):147–161, 2008.

375 [15] Takanori Hashimoto, H Holly Bazmi, Karoly Mirnics, Qiang Wu, Allan R Samp-
376 son, and David A Lewis. Conserved regional patterns of gaba-related transcript
377 expression in the neocortex of subjects with schizophrenia. *American Journal of*
378 *Psychiatry*, 165(4):479–489, 2008.

379 [16] Takanori Hashimoto, David W Volk, Stephen M Eggan, Karoly Mirnics, Joseph N
380 Pierri, Zhuoxin Sun, Allan R Sampson, and David A Lewis. Gene expression
381 deficits in a subclass of gaba neurons in the prefrontal cortex of subjects with
382 schizophrenia. *Journal of Neuroscience*, 23(15):6315–6326, 2003.

383 [17] Shuichi Isomura, Toshiaki Onitsuka, Rikako Tsuchimoto, Itta Nakamura, Shogo
384 Hirano, Yuko Oda, Naoya Oribe, Yoji Hirano, Takefumi Ueno, and Shigenobu
385 Kanba. Differentiation between major depressive disorder and bipolar disorder

- 386 by auditory steady-state responses. *Journal of affective disorders*, 190:800–806,
387 2016.
- 388 [18] Daniel C Javitt and Stephen R Zuckin. Recent advances in the phencyclidine
389 model of schizophrenia. *The American journal of psychiatry*, 1991.
- 390 [19] Joshua T Kantrowitz and Daniel C Javitt. N-methyl-d-aspartate (nmda) re-
391 ceptor dysfunction or dysregulation: the final common pathway on the road to
392 schizophrenia? *Brain research bulletin*, 83(3-4):108–121, 2010.
- 393 [20] Kübra Kömek, G Bard Ermentrout, Christopher P Walker, and Raymond Y Cho.
394 Dopamine and gamma band synchrony in schizophrenia—insights from computa-
395 tional and empirical studies. *European Journal of Neuroscience*, 36(2):2146–2155,
396 2012.
- 397 [21] Jun Soo Kwon, Brian F O’Donnell, Gene V Wallenstein, Robert W Greene, Yoshio
398 Hirayasu, Paul G Nestor, Michael E Hasselmo, Geoffrey F Potts, Martha E Shen-
399 ton, and Robert W McCarley. Gamma frequency–range abnormalities to auditory
400 stimulation in schizophrenia. *Archives of general psychiatry*, 56(11):1001–1005,
401 1999.
- 402 [22] David A Lewis, Allison A Curley, Jill R Glausier, and David W Volk. Cortical
403 parvalbumin interneurons and cognitive dysfunction in schizophrenia. *Trends in*
404 *neurosciences*, 35(1):57–67, 2012.
- 405 [23] David A Lewis, Takanori Hashimoto, and David W Volk. Cortical inhibitory
406 neurons and schizophrenia. *Nature Reviews Neuroscience*, 6(4):312–324, 2005.

- 407 [24] Chieh-Hsin Lin, Hsien-Yuan Lane, and Guochuan E Tsai. Glutamate signaling
408 in the pathophysiology and therapy of schizophrenia. *Pharmacology Biochemistry
409 and Behavior*, 100(4):665–677, 2012.
- 410 [25] Tuomo Maki-Marttunen, Tobias Kaufmann, Torbjorn Elvsashagen, Anna Devor,
411 Srdjan Djurovic, Lars T Westlye, Marja-Leena Linne, Marcella Rietschel, Dirk
412 Schubert, Stefan Borgwardt, et al. Biophysical psychiatry-how computational
413 neuroscience can help to understand the complex mechanisms of mental disorders.
414 2019.
- 415 [26] Christoph Metzner. [Re] Modeling GABA Alterations in Schizophrenia: A Link
416 Between Impaired Inhibition and Gamma and Beta Auditory Entrainment. *Re-
417 Science*, 3(1):6, August 2017.
- 418 [27] Christoph Metzner, Tuomo Mäki-Marttunen, Gili Karni, Hana McMahan-Cole,
419 and Volker Steuber. The effect of alterations of schizophrenia-associated genes on
420 gamma band oscillations. *bioRxiv*, 2020.
- 421 [28] Christoph Metzner, Tuomo Mäki-Marttunen, Bartosz Zurowski, and Volker Steu-
422 ber. Modules for automated validation and comparison of models of neurophysi-
423 ological and neurocognitive biomarkers of psychiatric disorders: Assrunit—a case
424 study. *Computational Psychiatry*, 2:74–91, 2018.
- 425 [29] Christoph Metzner, Achim Schweikard, and Bartosz Zurowski. Multifactorial
426 modeling of impairment of evoked gamma range oscillations in schizophrenia.
427 *Frontiers in computational neuroscience*, 10:89, 2016.

- 428 [30] Christoph Metzner, Bartosz Zurowski, and Volker Steuber. the role of
429 parvalbumin-positive interneurons in auditory steady-state response deficits in
430 schizophrenia. *Scientific Reports*, 9(1):1–16, 2019.
- 431 [31] Harvey M Morris, Takanori Hashimoto, and David A Lewis. Alterations in so-
432 matostatin mrna expression in the dorsolateral prefrontal cortex of subjects with
433 schizophrenia or schizoaffective disorder. *Cerebral Cortex*, 18(7):1575–1587, 2008.
- 434 [32] Linda S Overstreet and Gary L Westbrook. Synapse density regulates indepen-
435 dence at unitary inhibitory synapses. *Journal of Neuroscience*, 23(7):2618–2626,
436 2003.
- 437 [33] Bernhard Ross and Christo Pantev. Auditory steady-state responses reveal ampli-
438 tude modulation gap detection thresholds. *The Journal of the Acoustical Society
439 of America*, 115(5):2193–2206, 2004.
- 440 [34] Bernhard Roß, Terence W Picton, and Christo Pantev. Temporal integration in
441 the human auditory cortex as represented by the development of the steady-state
442 magnetic field. *Hearing research*, 165(1-2):68–84, 2002.
- 443 [35] Robert A Seymour, Gina Rippon, Gerard Gooding-Williams, Paul F Sowman,
444 and Klaus Kessler. Reduced auditory steady state responses in autism spectrum
445 disorder. *Molecular autism*, 11(1):1–13, 2020.
- 446 [36] Pascal Steullet, HC Neijt, Michel Cuénod, and KQ Do. Synaptic plasticity im-
447 pairment and hypofunction of nmda receptors induced by glutathione deficit:
448 relevance to schizophrenia. *Neuroscience*, 137(3):807–819, 2006.

- 449 [37] Hanna Thuné, Marc Recasens, and Peter J Uhlhaas. The 40-hz auditory steady-
450 state response in patients with schizophrenia: a meta-analysis. *JAMA psychiatry*,
451 73(11):1145–1153, 2016.
- 452 [38] Peter J Uhlhaas and Wolf Singer. Oscillations and neuronal dynamics in
453 schizophrenia: the search for basic symptoms and translational opportunities.
454 *Biological psychiatry*, 77(12):1001–1009, 2015.
- 455 [39] Julia Veit, Richard Hakim, Monika P Jadi, Terrence J Sejnowski, and Hillel
456 Adesnik. Cortical gamma band synchronization through somatostatin interneu-
457 rons. *Nature neuroscience*, 20(7):951, 2017.
- 458 [40] Dorea Vierling-Claassen, Peter Siekmeier, Steven Stufflebeam, and Nancy Kopell.
459 Modeling gaba alterations in schizophrenia: a link between impaired inhibition
460 and altered gamma and beta range auditory entrainment. *Journal of neurophys-*
461 *iology*, 99(5):2656–2671, 2008.
- 462 [41] Ikwunga Wonodi, O Colin Stine, Korrapati V Sathyasaikumar, Rosalinda C
463 Roberts, Braxton D Mitchell, L Elliot Hong, Yasushi Kajii, Gunvant K Thaker,
464 and Robert Schwarcz. Downregulated kynurenine 3-monooxygenase gene expres-
465 sion and enzyme activity in schizophrenia and genetic association with schizophre-
466 nia endophenotypes. *Archives of general psychiatry*, 68(7):665–674, 2011.
- 467 [42] Tsung-Ung Woo, Jed L Miller, and David A Lewis. Schizophrenia and the
468 parvalbumin-containing class of cortical local circuit neurons. *American Jour-*
469 *nal of Psychiatry*, 154(7):1013–1015, 1997.